JOURNAL OF CATALYSIS **168,** 501–510 (1997)
ARTICLE NO. CA971651

Catalytic Hydrogenolysis of 1,1,2-Trichlorotrifluoroethane on γ-Al_2O_3-Supported Palladium/Zinc Oxide Catalyst

S. P. Scott,* M. Sweetman,* J. Thomson,*,[1] A. G. Fitzgerald,† and E. J. Sturrock†

*Department of Chemistry and †Department of Applied Physics and Electronics and Mechanical Engineering, University of Dundee, Dundee, DD1 4HN, Scotland, United Kingdom

Received November 19, 1996; revised February 3, 1997; accepted February 3, 1997

The catalytic hydrogenolysis of 1,1,2-trichlorotrifluoroethane on a γ-alumina-supported palladium/zinc oxide catalyst under flow conditions has been conducted. The results show that relative to a γ-alumina-supported palladium system, enhanced conversion of the feedstock is achieved to give a mixture of chlorofluorohydrocarbons and hydrofluoroalkanes. Kinetic studies show that the addition of zinc to the palladium metal function alters the equilibrium for the hydrogenolysis reaction, giving higher selectivity to dechlorinated products. The lifetime of the Pd/ZnO/γ-Al_2O_3 catalyst is also enhanced relative to a Pd/γ-Al_2O_3 system operating under identical conditions. Differential scanning calorimetry, X-ray diffraction, X-ray photoelectron spectroscopy (XPS), and kinetic analysis indicate a synergistic relationship between the palladium and zinc(II) oxide functions, where a zinc-rich phase evokes chemical stability and increased dispersion upon discrete metallic palladium crystallites. XPS analysis of the palladium and zinc functions respectively shows that catalyst deactivation occurs through the formation of palladium(IV) halide in conjunction with palladium enrichment of the surface.

INTRODUCTION

Since the mid-seventies a great deal of research in the field of catalytic fluorine chemistry has been directed towards addressing the problem of ozone depletion, in which chlorofluorocarbons are implicated, although their ozone depletion potential is a fraction of that of chlorocarbons or bromochlorocarbons (1). Hence the chlorofluorocarbon industry has directed much of its research towards the manufacture of materials to replace chlorofluorocarbons (2–14). Among the many patented preparations for the production of these materials is the catalytic conversion of chlorofluorocarbons by hydrogenolysis to chlorofluorohydrocarbons or hydrofluoroalkanes (15–29). However, the reaction is a challenging task for heterogeneous catalysis owing to the oxidising conditions prevalent at high temperatures within the reactor through the *in situ* generation of gaseous hydrogen fluoride and hydrogen chloride. These gaseous by-products subsequently attack the metal function and/or the oxide support material, resulting in a loss of both the metal and the support areas (30).

Hydrogenolysis of the carbon–halogen bond using metals has long been studied, but relatively few studies have dealt with the hydrogenolysis of chlorofluorocarbons (31–33). The most efficient metals for the hydrogenolysis reaction of chlorofluorocarbons are palladium and platinum (22, 34, 35). The most widely used catalysts for the hydrogenolysis of chlorine are carbon-supported or aluminium(III) fluoride-supported palladium, which operate at temperatures between 500 and 773 K at pressures at, and above, atmospheric (36). The stability and selectivity of these catalyst systems vary, with the aluminium(III) fluoride-supported palladium exhibiting enhanced catalytic lifetime relative to that of the carbon-supported palladium system (37). However, both these catalysts are prone to accelerated deactivation during the early stages of their reactor life, with a loss in activity of up to 50% over the first 20 h (30). This loss in activity is coupled with a dramatic decrease in the extent of dechlorination of the chlorofluorocarbon and hence a reduction in the selectivity of the catalyst to hydrofluoroalkanes. The loss in hydrogenolysis activity has been shown to be caused by the formation of nonlabile halogen at the metal function, reducing the metal area for the subsequent dissociative chemisorption of the dihydrogen and chlorofluorocarbon substrates. The formation of the nonlabile halogen adsorbates results in the oxidation of palladium from its initial metallic state.

We report the results of a study directed towards improving the catalytic activity and selectivity to hydrofluoroalkanes, for the hydrogenolysis of 1,2,2-trichlorotrifluoroethane using a T_2–B_1 (second row transition metal coupled to Group B metal) catalyst system (9, 13), and examining the role of the B_1 metal function in the catalyst formulation. To give the study a mechanistic insight, hydrogenolysis of 1,1,2,-trichlorotrifluoroethane was selected as the probe reaction, owing to the variation in the chlorine and fluorine content of the α and β carbons, respectively. The study also examines the physical stability of the T_2 and B_1 metal

[1] To whom correspondence should be addressed.

0021-9517/97 $25.00

functions, respectively, during deactivation of a Pd/ZnO/γ-alumina system under flow conditions.

EXPERIMENTAL

A 5 wt% by palladium, γ-alumina-supported Pd/ZnO catalyst (1 g, Degussa "C", sample area 110 $m^2\ g^{-1}$; Pd/Zn ratio 1 : 2) was prepared by wet impregnation, using palladium nitrate hydrate (0.108 g, 0.47 mmol, Aldrich Chemical Co.) and zinc(II) oxide (0.08 g, 0.94 mmol, BDH Chemicals). Catalysts were prepared with varying Pd/ZnO ratios, the palladium loading being held constant. Catalyst A has a Pd/ZnO ratio of 2 : 1, B = 1 : 1, C = 1 : 2, and D = 1 : 4; catalyst E is γ-alumina-supported zinc(II) oxide; and catalyst F is a 5 wt% loading of γ-alumina-supported palladium. Metal ion-impregnated samples were dried under a flow of oxygen free dinitrogen (30 $cm^3\ min^{-1}$) at 523 K over a 2-h period, followed by calcination in air at 523 K for 2 h. The reactor was flushed with dinitrogen for 30 min, during which the reactor temperature was reduced to 323 K. Reduction of the samples was performed in a 10% H_2/N_2 feedstream (flowrate, 44 $cm^3\ min^{-1}$). The reduction temperature was ramped at 2°C min^{-1} and held at 373, 423, 473, 523, and 573 K, respectively, over a 30-min period. The reactor temperature was finally increased to 623 K and held under a H_2/N_2 flow for a further 2 h prior to reducing the reactor temperature under a H_2/N_2 flow to 500 K.

Dry oxygen free nitrogen was bubbled through a reservoir of 1,1,2-trichlorotrifluoroethane (Aldrich Chemical Co.; HPLC Grade > 99.99% purity; flowrate, 13.5 $cm^3\ min^{-1}$) at ambient temperatures to give a time-averaged feedrate of 43 μl min^{-1}. Dry oxygen free hydrogen (purity > 99.9%) was set to 6 $cm^3\ min^{-1}$. The reactor pressure was held constant at 900 Torr over the temperature range 340–700 K, and dihydrogen flow was set to give a 10% H_2/N_2 ratio. Reactor space velocity was set at 1800 h^{-1}. The reactor eluent was analysed using a Carbopak column with nitrogen carrier. The retention times and calibration of the G/C data were performed using authentic samples of 1,1,2-trichlorotrifluoroethane, 2,2-dichlorotrifluoroethane, 2-chlorotrifluoroethane, and 1,1,1-trifluoroethane (Aldrich Chemical Co.).

Catalyst samples were also examined by X-ray photoelectron spectroscopy (XPS), using a VG HB 100 Multilab system equipped with a concentric hemispherical analyser (CHA). Al$K\alpha$ monochromatic X rays (1486 eV) were used to generate the spectra. Correction for binding energies owing to sample charging was effected by taking the C_{1s} line at 284.6 eV as the internal standard. Quantitative analyses of the XPS data were performed with the intensities of the peaks using QUAX software (38). X-ray diffraction (XRD) experiments were performed using a Philips PW 1010 X-ray generator fitted with a PW 2213/20 1.5 kW copper tube running at 40 kV. Differential scanning calorimetric (DSC) data were obtained using a Mettler Toledo TA8000 thermal analysis system fitted with a Mettler DSC 25 module. Prepared catalyst samples were analysed by DSC in an environment of air or nitrogen as appropriate.

RESULTS

Samples of catalyst 5 wt% Pd/γ-Al_2O_3, ZnO/γ-Al_2O_3, and Pd/ZnO/γ-Al_2O_3 (Pd/ZnO ratio 1 : 2) were prepared and analysed using XRD and XPS procedures as described under Experimental. Although the catalyst samples were all reduced prior to analysis, no special procedures were taken to avoid the exposure of the samples to air during XRD and XPS sample loading. XRD analysis of the treated γ-Al_2O_3-supported zinc(II) oxide sample gave 2θ peaks at 31.7°, 36.1°, 47.5°, 56.5°, 62.9°, and 68.1° and confirms the presence of a bulk zinc(II) oxide phase after the reduction procedure (39). XPS analysis gives a $Zn_{2p\,3/2}$ binding energy of 1024.4 eV which is consistent with a zinc function being in a Zn^{2+} state (40). These results confirm that for γ-alumina-supported zinc(II) oxide material, the pretreatment stage does not reduce the zinc(II) oxide phase of the supported catalyst. The zinc(II) oxide/γ-Al_2O_3 system exhibits no activity for hydrogenolysis of 1,1,2-trichlorotrifluoroethane. Instead a mixture of zinc(II) chloride is eluted from the reactor through the temperature range 433–470 K.

XRD analysis of the Pd/γ-Al_2O_3 and the Pd/ZnO/γ-Al_2O_3 samples, respectively (Pd/ZnO ratio 1 : 2), shows that Pd/γ-Al_2O_3 gives peaks at 2θ values of 40.1°, 46.6°, and 67.9° and confirms the presence of bulk palladium crystallites in the treated sample (39). Conversely, the Pd/ZnO/γ-Al_2O_3 sample, prepared under identical reduction conditions, shows no evidence of bulk palladium, zinc, or zinc(II) oxide; however, new peaks at 2θ values of 40.10° and 43.95° are observed, which is consistent with the formation of a palladium–zinc phase (41). XPS sample analysis is consistent with Pd/Zn/γ-Al_2O_3 being in a fully reduced state with the $Pd_{3d\,5/2}$ binding energy of 335.1 eV (Table 1). XRD analysis shows no evidence of bulk crystalline palladium(II) oxide. Hence, palladium contained in the Pd/ZnO/γ-Al_2O_3 sample is either in an amorphous phase, extremely small crystallite form, or alloyed with the zinc function to give a new phase. Cell dimension calculations from the 2θ peaks obtained from the Pd/ZnO/γ-Al_2O_3 material give a cubic structure with a cell dimension of 7.94 Å. The addition of zinc oxide to the precursor sample preparation (Pd/ZnO ratio 1 : 2) reduces the $Pd_{3d\,5/2}$ electron binding energy from 335.5 to 335.15 eV and shows that the presence of zinc in the catalyst formulation results in the palladium metal environment being electronegative and in a highly dispersed state relative to the Pd/γ-alumina system (42). It should be noted that the electron binding energy of the zinc function is also in a reduced state relative to the zinc oxide/γ-alumina material (Table 1). The presence of palladium catalyses the

TABLE 1

XPS Data from Sample Analysis (Binding Energy eV)

	Pd-3$d_{(5/2)}$	Zn-2$p_{(3/2)}$	Al-2$s_{(1/2)}$	Pd/Zn peak ratio	Zn/Al peak ratio	Pd/Al peak ratio
Pd/alumina sample	335.50	0.00	119.6	0.0000	0.000	0.1558
ZnO/alumina sample	0.00	1024.40	120.5	0.0000	2.087	0.0000
Fresh Pd/ZnO/alumina	335.15	1022.65	119.6	0.0320	1.984	0.0637
F-Pd/ZnO/alumina	337.00	1023.60	120.2	0.1006	0.940	0.0946

Note. Reference, C_{1s} 284.6 eV.

reduction of zinc(II) oxide during the pretreatment stage. The electron binding energy of the $Zn_{2p\ 3/2}$ electron is shifted down from 1024.40 to 1022.65 eV for the Pd/ZnO/γ-Al_2O_3 material. The electron binding energy of the $Zn_{2p\ 3/2}$ electron in the pure metal is reported to be 1020.8 eV (40).

The hydrogenolysis activity for the 5 wt% Pd/γ-Al_2O_3 system results in an 11% conversion of 1,1,2-trichlorotrifluoroethane to 1,1,1-trifluoroethane (Table 2) with deactivation of the catalyst proceeding at a rate of 2.5 conversion % h^{-1}. At low conversions second-order kinetics are displayed for 1,1,2-trichlorotrifluoroethane consumption to give an apparent energy of activation (E_{app}) of 61.4 kJ mol^{-1} (Fig. 1) and a rate constant of 1.3 μmol min^{-1} g-catalyst^{-1} at 653 K. This measured activation energy for the system will include the heats of adsorption for 1,1,2-trichlorotrifluoroethane and dihydrogen, respectively.

Results of the hydrogenolysis of 1,1,2-trichlorotrifluoroethane on catalyst A (Pd/ZnO 2 : 1, Table 2) show that conversions of ca. 8–20 mol% are obtained across the temperature range 503–653 K, giving the major product 1,1-dichloro-2,2,2-trifluoroethane (54 mol%), followed by 1-chloro-2,2,2-trifluoroethane (15 mol%). The selectivity to 1,1,1-trifluoroethane varies with temperature at around 2 mol%. Hydrogenolysis of chlorine from 1,1,2-trichlorotrifluoroethane is low at only 3% (Table 2). The E_{app} for the reaction is 64.0 kJ mol^{-1} (Fig. 1), and the rate of catalyst deactivation was measured as 2.5 conversion % h^{-1}. The deactivation rate is similar to that of the Pd/γ-Al_2O_3 system.

Hydrogenolysis of 1,1,2-trichlorotrifluoroethane on catalyst B (Pd/ZnO ratio 1 : 1) as a function of temperature gives conversions of 1,1,2-trichlorotrifluoroethane up to 42.9% over the temperature range 550–663 K. Activity is increased relative to that obtained for catalyst A over the same temperature range. Selectivity to 1,1,1-trifluoroethane is also increased to 9.0 mol% at 643 K, prior to an exponential increase to 67.7 mol% at 673 K. 1,1-Dichloro-2,2,2-trifluoroethane appears as a minor product in the reactor

TABLE 2

Product Distribution from Hydrogenolysis of 1,1,2-Trichlorotrifluoroethane

Catalyst	Temp (K)	Conversion %	CH_3CF_3 (mol%)	CH_2ClCF_3 (mol%)	$CHCl_2CF_3$ (mol%)	Others (mol%)	% Chlorine removal
Pd/Zn ratio 2 : 1	503	7.19	10.83	18.94	54.14	16.08	2.8
	553	8.39	4.81	17.34	58.04	19.81	3.0
	603	10.09	3.22	11.45	57.21	28.10	3.0
	653	19.79	2.67	2.67	34.66	60.00	3.2
Pd/Zn ratio 1 : 1	553	15.99	38.82	59.76	1.42	0.00	12.6
	603	12.91	15.34	82.53	2.13	0.00	9.1
	643	19.06	8.95	83.16	5.26	2.63	12.6
	658	20.58	30.23	59.17	5.42	5.17	14.7
	663	42.90	64.45	22.07	7.38	6.10	34.8
	673	49.90	67.72	14.40	10.15	7.73	49.2
Pd/Zn ratio 1 : 2	548	5.62	99.32	0.68	0.00	0.00	5.6
	573	9.18	88.55	11.45	0.00	0.00	8.8
	589	8.22	85.89	14.03	0.00	0.09	7.8
	633	10.69	69.12	16.90	13.08	0.08	9.0
	648	18.52	43.95	44.04	11.01	1.00	14.2
	673	66.14	29.38	64.26	6.10	0.25	49.1
Pd/Zn ratio 1 : 4	553	61.93	98.41	0.00	1.59	0.00	61.3
	603	77.14	98.11	0.55	1.26	0.00	76.3
	653	83.13	97.00	1.86	1.14	0.00	81.9
	673	83.85	93.77	4.42	1.81	0.00	81.6

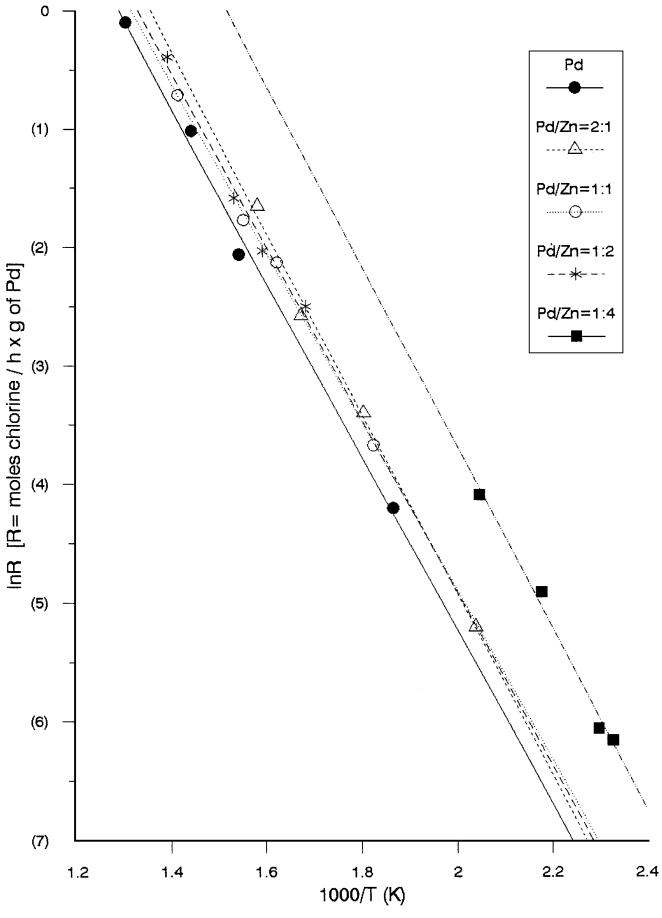

FIG. 1. Arrhenius plot of 1,1,2-trichlorotrifluoroethane specific rate as a function of palladium content for various ratios of γ-alumina–supported Pd/ZnO.

eluent during the initial stages of the reaction at ca. 2 mol%. At lower conversions, the selectivity to CH_2ClCF_3 is greater than that of catalyst A at 59 mol%. However, selectivity to CH_2ClCF_3 decreases as the reaction temperature moves through the temperature range 600–673 K. The efficiency of the catalyst in removing chlorine was also increased over catalyst A at 49.2%. Deactivation of catalyst B proceeds with a loss in conversion of 0.9% h^{-1}. First-order kinetics for CCl_2FCClF_2 consumption are also observed at temperatures up to 653 K, with an E_{app} for hydrogenolysis of 60.0 kJ mol^{-1} (Fig. 1).

The conversion and selectivity of catalyst C as a function of temperature for the hydrogenolysis of 1,1,2-trichlorotrifluoroethane show that as the reaction temperature is increased, the system exhibits increasing reactivity relative to the γ-Al_2O_3-supported palladium and the Pd/Zn ratio = 2 : 1, materials respectively, to give conversions up to 66% at 673 K. At higher temperatures halogenation of the alumina support by 1,1,2-trichlorotrifluoroethane results in the formation of aluminium(III) fluoride. XRD analysis of the worked material shows the presence of 2θ bands at 3.55°, 3.13°, 2.06°, 1.77°, and 1.59°, confirming the formation of AlF_3 by the support (39). XPS analysis of a deactivated catalyst shows that the palladium metal function is oxidised to Pd^{4+} to give a $Pd_{3d\ 5/2}$ electron binding energy of 337.0 eV (43, 44) (Table 1). Peak area analysis also confirms that palladium enrichment of the surface material occurs during deactivation with the Pd/Zn peak ratios increasing from 0.03 to 0.10, and the Pd/Al peak ratio increases from 0.06 to 0.09, an increase of 48.5%. Correspondingly, the relative peak ratio of Zn/Al is reduced as a function of catalyst operation from 2.0 to 0.9, a decrease of 52.6%, and is consistent with a depletion or elution of zinc from the catalyst surface.

DSC analysis was performed in air and the results are shown for net influence of the zinc component in the Pd/ZnO/γ-alumina system (Pd/Zn 1 : 2, catalyst C), relative to that of the 5 wt% Pd/γ-alumina material (Fig. 2). The DSC results show that for temperatures between 496 and 575 K, the system exhibits an exothermic profile maximising at 3.2 kJ (g of catalyst)$^{-1}$ at 573 K. This shows that over this temperature range, the palladium metal function is less stable to oxidation relative to the Pd/γ-Al_2O_3 standard. However, from 576 to 610 K, the palladium metal function of a Pd/ZnO system exhibits an endothermic profile relative to the Pd/γ-alumina material. Maximum stability is shown over this temperature range where the material is more stable to oxidation relative to the Pd/γ-Al_2O_3 system by 9.0 kJ (g of catalyst)$^{-1}$.

For the Pd/Zn = 1 : 2 system, at 548 K a low conversion of 1,1,2-trichlorotrifluoroethane occurs with high selectivity to 1,1,1-trifluoroethane. As the reactor temperature is increased to 573 K, 1-chloro-2,2,2-trifluoroethane appears in the reactor eluent, and increases as a function of temperature until at temperatures above 650 K, CH_2ClCF_3 becomes the major component with a molar ratio of 64 mol%. At the temperature of 648 K, conversion of CCl_2FCClF_2 is dramatically increased from ca. 19 to 66%. Infrared analysis of the reaction by-products identifies the presence of SiF_4 (generated from the reaction of gaseous hydrogen fluoride with the Pyrex glass) with gaseous hydrogen chloride also present. It should be noted that the products 1,2,2-trifluoroethane or 1-chloro-1,2,2-trifluoroethane are not detected as reaction products, and this indicates that an isomerisation process is operating during the reaction to form a terminal $-CF_3$ group. The formation of 1,1,1-trichlorotrifluoroethane is thermodynamically stable by 39 kJ mol^{-1} over the formation of 1-chloro-2,2 dichlorotrifluoroethane (45). Deactivation of catalyst C occurs with a loss in the conversion of 1,1,2-trichlorotrifluoroethane at a rate of 0.6% h^{-1}, a value lower than that obtained for the Pd/γ-Al_2O_3 system. Efficiency in chlorine removal for the catalyst formulation is shown to be 49.1% at the reaction temperature of 673 K. The rate constant for consumption

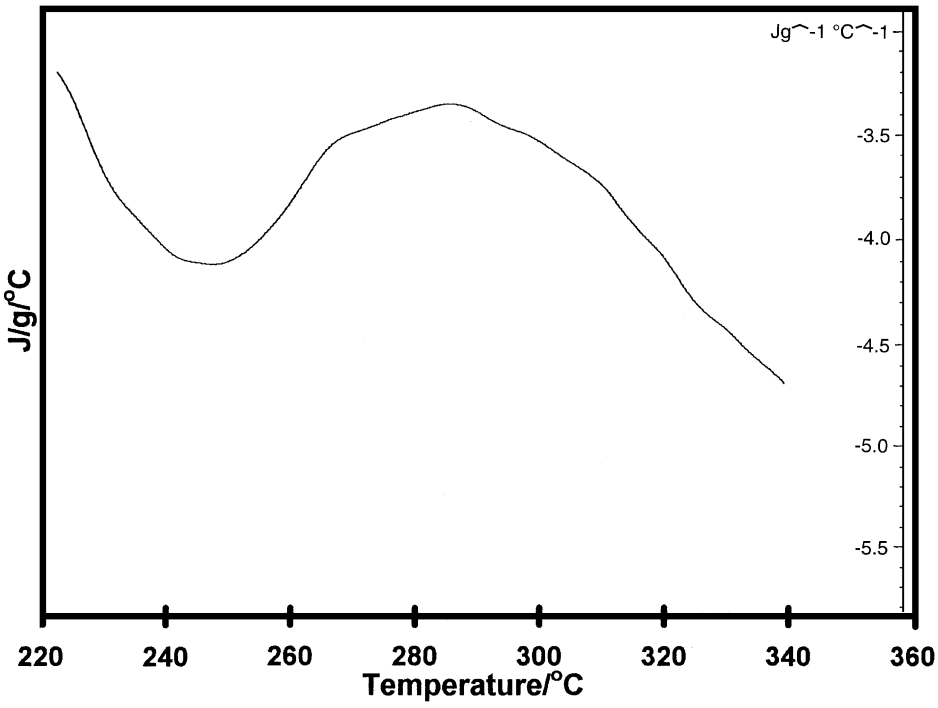

FIG. 2. DSC scan difference for Pd/Zn/γ-alumina–Pd/γ-alumina samples (same sample mass).

of CCl_2FCClF_2 is 6.3 μmol min^{-1} g-catalyst^{-1}, and the E_{app} for hydrogenolysis is 61.3 kJ mol^{-1} (Fig. 1).

Reducing the Pd/ZnO ratio to 1:4 (catalyst D) dramatically increases the conversion of 1,1,2-trichlorotrifluoroethane during hydrogenolysis (Table 1) and an E_{app} of 64.1 kJ mol^{-1} (Fig. 1). At the reaction temperature of 553 K conversion is recorded at 61.9% with a selectivity to 1,1,1-trifluoroethane of 98 mol%. The high conversion for this formulation corresponds to conversions of 7 and 16% for catalysts A and B, respectively, operating under the same reaction conditions. Increasing the temperature of the reaction to 673 K results in a small reduction in the selectivity to 1,1,1-trifluoroethane with 4.4 mol% of 1-chloro-2,2,2-trifluoroethane being produced (Table 1). Catalyst D exhibits the best selectivity to 1,1,1-trifluoroethane over the range of Pd/ZnO ratios examined and has a chlorine removal efficiency of 81%. The rate of deactivation for catalyst D was 0.5% conversion h^{-1} and shows that the palladium function exhibits a high resistance to oxidation in the presence of gaseous HX (X = Cl or F) at elevated temperatures during the reaction.

DISCUSSION

The industrial preparation of 1,1,1,2-tetrafluoroethane under catalytic conditions can be achieved by the hydrogenolysis of 1,1-dichlorotetrafluoroethane on carbon-supported or aluminium(III) fluoride-supported palladium, respectively (30). Deactivation of the catalyst can occur by the adsorption of halogen (fluorine and chlorine) at the palladium surface, and/or halogenation of oxide support if used, with the resultant loss in the support BET area, inducing sintering of the metal function. Under hydrogenolysis conditions of high temperatures where copious quantities of gaseous hydrogen fluoride and hydrogen chloride can be generated, oxidation of the metal leads to the formation of palladium(IV) halides.

X-ray diffraction results of the Pd/γ-Al_2O_3 system confirm the presence of palladium crystallites exhibiting bulk crystalline properties. XPS analysis of the Pd/γ-Al_2O_3 shows that the $Pd_{3d\,5/2}$ electron binding energy of 335.5 eV confirms that the metal is in an electropositive state compared to that of Pd^0 which has a binding energy of 335.2 eV (40, 43, 44). XRD analysis of the freshly prepared Pd/ZnO/γ-Al_2O_3 (Pd/Zn = 1:2), treated under identical reduction procedures, shows a 54.7% reduction in the intensity of the 2θ peak assigned to palladium crystallites with a peak width at half-peak height increasing by 0.0145 radian. The Scherrer equation (46) suggests that the mean particle diameter of the crystallites is reduced from 6.9 to 4.4 nm, respectively. This indicates that the palladium metal dispersion is (a) in a finely dispersed state, (b) is amorphous in character, or (c) is a component in a non-crystalline material comprising the catalyst surface. XRD data from the Pd/Zn/γ-Al_2O_3 (Pd/Zn = 1:2) show the presence of 2θ peaks at 40.1 and 44.0 which is consistent with

a Pd/Zn alloy (41). XPS data show that the $Pd_{3d\,5/2}$ binding energy of the Pd/Zn material is 335.15 eV, a value confirming that palladium is electronegative with respect to the Pd/γ-Al_2O_3 sample. XRD and XPS analyses of a γ-Al_2O_3-supported zinc(II) oxide treated under identical reduction conditions confirm that no reduction of the zinc oxide material occurs. XPS analysis of the ZnO/γ-Al_2O_3 gives the $Zn_{2p\,3/2}$ binding energy of 1024.4 eV, and 1022.7 eV for the freshly prepared Pd/ZnO/γ-Al_2O_3. The $Zn_{2p\,3/2}$ binding energy for the ZnO/γ-Al_2O_3 sample confirms that the zinc function is in a Zn^{2+} state (40). The presence of palladium catalyses the reduction of zinc(II) oxide, resulting in zinc-rich phase relative to the γ-Al_2O_3-supported zinc(II) oxide system, with the result that the palladium function is electronegative by 0.4 eV relative to Pd/γ-Al_2O_3 and 0.1 eV relative to palladium metal. The reduction of the zinc(II) oxide phase in the presence of palladium is consistent with hydrogen spillover from a reduced palladium region. The results suggest that the palladium crystallites are highly dispersed, and in intimate contact with material being of reducing character, i.e., metallic zinc. Comparison of the Pd/Al peak ratios from the Pd/γ-Al_2O_3 and the fresh Pd/ZnO/γ-Al_2O_3 samples, respectively, shows a 2.5-fold reduction in the photoelectron density from $Pd_{3d\,5/2}$, which is consistent with a Pd/ZnO ratio of 1 : 2 where 1/3 of surface atoms are palladium. The XPS results indicate that the palladium metal is uniformly dispersed through a matrix of zinc. The Zn/Al ratio for the sample is unchanged for the γ-Al_2O_3-supported zinc(II) oxide and the freshly prepared Pd/ZnO/γ-Al_2O_3, respectively (Table 1). Therefore the XPS results indicate that the zinc-rich phase is also highly dispersed and is consistent with the XRD analysis which shows that zinc(II) oxide material is not present.

Kinetic analysis of the 1,1,2-trichlorotrifluoroethane consumption on the Pd/γ-Al_2O_3 material gives an E_{app} of 69.2 kJ mol^{-1} which is comparable with the E_a for 1,1-dichloromethane hydrogenolysis (30). Studies of the production of CH_3CF_3 show second-order kinetics at low surface coverage of CCl_2FCClF_2 with the substrate and product compounds being held weakly at the surface. A conversion of 11% with a selectivity of 94% to 1,1,1-trifluoroethane is obtained for the reaction. Infrared analysis of the eluent gases confirms the presence of gaseous HCl and HF. The efficiency of Pd/γ-Al_2O_3 in removing chlorine is measured at 5% with a time average deactivation in conversion of 2.9% h^{-1}.

Kinetic analysis of the Pd/ZnO/γ-Al_2O_3 system (Pd/Zn = 2 : 1) gives conversions in the range of 10–20%, i.e., values similar to that obtained for the Pd/γ-Al_2O_3 system (Table 1). However, the selectivity to CH_3CF_3 was markedly lower at ca. 3 mol% compared with that observed for the Pd/γ-Al_2O_3 system. Loss in selectivity to 1,1,1-trifluoroethane is measured at 0.1 mol% K^{-1} between the temperatures 500 and 600 K. The changing selectivity over this temperature range indicates that the catalyst surface is undergoing change, owing to (i) a restructuring of the surface, (ii) the adsorption of nonlabile adsorbates, or (iii) variable surface coverages of adsorbate species. Above 600 K no loss in selectivity to 1,1,1-trifluoroethane as a function of temperature is observed, which indicates that the catalyst surface has reached structural stability or steady state conditions in adsorbate equilibrium. The Arrhenius plot for consumption of 1,1,2-trichlorotrifluoroethane gives an E_{app} for the reaction at 61.4 kJ mol^{-1}. The high molar ratio of 1,1-dichloro-2,2,2-trifluoroethane in the eluent shows the inefficiency of the catalyst to effect full hydrogenolysis of chlorine from 1,1,2-trichlorotrifluoroethane through to 1,1,1-trifluoroethane. The extent of chlorine hydrogenolysis is shown to be a function of the reaction temperature. As the reaction temperature is increased the molar ratio of chlorine containing compounds is reduced, with a corresponding increase in the partial pressure of gaseous hydrogen chloride and hydrogen fluoride eluting from the reactor (Table 2). XRD analysis of the worked catalyst confirms the formation of aluminium(III) fluoride, and examination of the apparatus shows the build up of aluminium(III) chloride downline from the reactor. The formation of aluminium(III) halides from the support material results in a loss of support area with subsequent sintering of the metal function and a corresponding loss in catalyst activity. The presence of $HCl_{(g)}$ and $HF_{(g)}$ gives an insight into the mechanism occurring at the catalyst surface during the hydrogenolysis reaction (Fig. 3). Product analysis shows that only the asymmetric compound is eluted from the reactor, and the formation of the terminal $-CF_3$ group must be taken into account in any reaction scheme that is proposed. The efficiency of the system to remove chlorine is ca. 3%, and deactivation of the catalyst was similar to that of Pd/γ-Al_2O_3 at 2.5% h^{-1}. The shift in the major product from 1,1,1-trifluoroethane for the Pd/γ-Al_2O_3 catalyst to 1,1-dichloro-2,2,2-trifluoroethane for the Pd/ZnO/γ-Al_2O_3 system (Pd/Zn = 2 : 1) shows that the addition of zinc to the palladium function affects the ability of the catalyst to push the hydrogenolysis reaction to completion. The chemical equilibria of the adsorbed species is affected owing to the addition of zinc, such that K_{eq} for the reaction favours $CHCl_2CF_3$ as the major product.

Increasing the zinc loading of the catalyst to give a Pd/Zn ratio of 1 : 1 produces an increase in the efficiency of the catalyst to remove chlorine from 1,1,2-trichlorotrifluoroethane to ca. 42% at 663 K with a corresponding shift in the major product from $CHCl_2CF_3$ to 1-chloro-2,2,2-trifluoroethane (CH_2ClCF_3). The addition of zinc to the catalyst has enhanced the ability of the surface to remove chlorine from the feedstock 1,1,2-trichlorotrifluoroethane. We can represent the

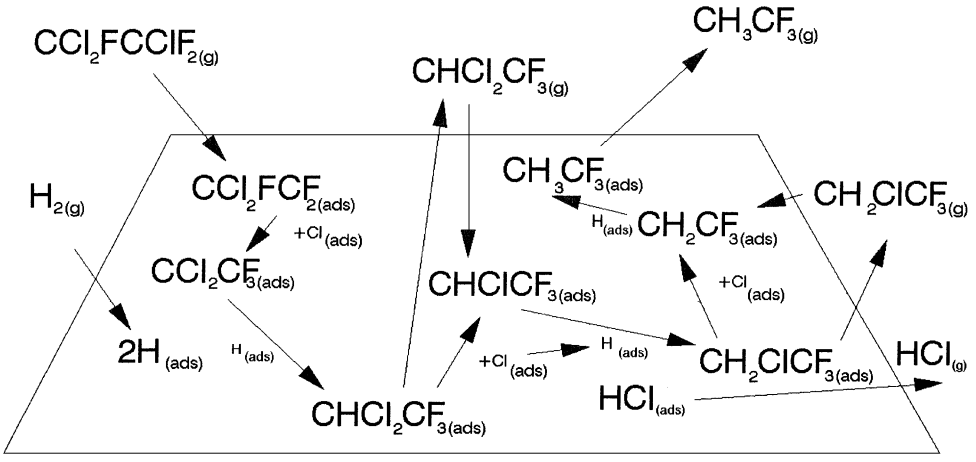

FIG. 3. Scheme of hydrogenolysis reaction of 1,1,2-trichlorotrifluoroethane.

hydrogenolysis of 1,1,2-trichlorotrifluoroethane as

$$CCl_2FCClF_{2(g)} \underset{\lambda_{-1}}{\overset{\lambda_1}{\rightleftharpoons}} CCl_2FCClF_{2(ads)} \qquad \Lambda_1 = \lambda_1/\lambda_{-1}$$

$$CCl_2FCClF_{2(ads)} \underset{k_{-1}}{\overset{k_1}{\rightleftharpoons}} CCl_3CF_{3(ads)} \qquad K_1 = k_1/k_{-1}$$

$$H_{2(g)} \underset{\lambda_{-2}}{\overset{\lambda_2}{\rightleftharpoons}} 2H_{(ads)} \qquad \Lambda_2 = \lambda_2/\lambda_{-2}$$

$$CCl_3CF_{3(ads)} + H_{(ads)} \underset{k_{-2}}{\overset{k_2}{\rightleftharpoons}} CHCl_2CF_{3(ads)} + HCl_{(ads)} \qquad K_2 = k_2/k_{-2}$$

$$CHCl_2CF_{3(ads)} \underset{\lambda_{-3}}{\overset{\lambda_3}{\rightleftharpoons}} CHCl_2CF_{3(g)} \qquad \Lambda_3 = \lambda_3/\lambda_{-3}$$

$$CHCl_2CF_{3(ads)} + H_{(ads)} \underset{k_{-3}}{\overset{k_3}{\rightleftharpoons}} CH_2ClCF_{3(ads)} + HCl_{(ads)} \qquad K_3 = k_3/k_{-3}$$

$$CH_2ClCF_{3(ads)} \underset{\lambda_{-4}}{\overset{\lambda_4}{\rightleftharpoons}} CH_2ClCF_{3(g)} \qquad \Lambda_4 = \lambda_4/\lambda_{-4}$$

$$CH_2ClCF_{3(ads)} + H_{(ads)} \underset{k_{-4}}{\overset{k_4}{\rightleftharpoons}} CH_3CF_{3(ads)} + HCl_{(ads)} \qquad K_4 = k_4/k_{-4}$$

$$CH_3CF_{3(ads)} \underset{\lambda_{-5}}{\overset{\lambda_5}{\rightleftharpoons}} CH_3CF_{3(g)} \qquad \Lambda_5 = \lambda_5/\lambda_{-5}$$

$$HCl_{(ads)} \underset{\lambda_{-6}}{\overset{\lambda_6}{\rightleftharpoons}} HCl_{(g)} \qquad \Lambda_6 = \lambda_6/\lambda_{-6}$$

where Λ_x and K_x are the gas phase equilibrium coefficients and reaction equilibrium coefficients, respectively.

At low partial pressure and low conversion of 1,1,2-trichlorotrifluoroethane, where surface coverage $\theta_{CCl_2FCClF_2}$ tends to zero, the rate of product formation being detected in the gas phase displays second-order kinetics. Under these conditions the generation of 1,1,1-trifluoroethane can be given as

$$\frac{d[CH_3CF_3]}{dt} = \frac{k_{\text{rate constant}} K_1 K_2 K_3 K_4 p_{CCl_2FCClF_2} p_{H_2}^{0.5}}{\left\{\left(1 + \Lambda_1 K_1 p_{CCl_2FCClF_2} + \Lambda_2 p_{H_2}^{0.5} + \Lambda_3 p_{CHCl_2CF_3} + \Lambda_4 p_{CH_2ClCF_3} + \Lambda_5 p_{CH_3CF_3} + \Lambda_6 p_{HCl}\right)\right\}^2}. \quad [1]$$

However, the above equation does not address the generation of anhydrous hydrogen fluoride during the reaction. Hydrogen fluoride generation can be accounted for by examining the isomerisation mechanism from 1,1,2-trichlorotrifluoroethane to 1,1,1-trichlorotrifluoroethane. Previous studies of the reaction of 1,1,2-trichlorotrifluoroethane in the presence of anhydrous hydrogen fluoride on chromia have suggested that isomerisation of 1,1,2-trichlorotrifluoroethane occurs in the gas phase (47). However, in the case of the reaction studied here the generation of hydrogen fluoride and the observation of the formation of terminal $-CF_3$ groups in the reaction products are consistent with a surface-induced isomerisation mechanism during dissociative chemisorption of 1,1,2-trichlorotrifluoroethane to give Cl_{ads} and $CF_2CFCl_{2(ads)}$ as surface species (Fig. 3). The presence of two fluorine atoms at an α-carbon induces an electropositive charge at the α-carbon. Fluorine at the β-carbon transfers to the α-carbon by a 1,2 shift forming the terminal trifluoromethyl group, resulting in a positive charge over the β-carbon. Surface-adsorbed chlorine can react to form a trichloromethyl group completing the isomerisation mechanism. Alternatively, the terminal fluorine comprising the dichlorofluoromethyl group of the β-carbon can be protonated by surface-adsorbed hydrogen during the intramolecular fluorine transfer mechanism to form hydrogen fluoride. However, before the above equation is modified to account for the formation of surface-adsorbed hydrogen fluoride there are a few other aspects of the reaction that must be considered.

Selectivity to 1,1,1-trifluoroethane is shown to decrease as a function of temperature at a rate of 0.5 mol% K^{-1} over the temperature range 550–620 K and this observation suggests changes in surface structure or surface coverage of adsorbates. At temperatures above 630 K the selectivity to

1,1,1-trifluoroethane remains constant over the duration of the experiment and is consistent with the reaction occurring on a stable surface. The E_{app} for the reaction is measured at 60.0 kJ mol^{-1} (Fig. 1), with a chlorine removal efficiency of ca. 49% at 673 K. An increase in the zinc content of the catalyst to give a Pd/Zn ratio of 1 : 2 does not substantially increase the chlorine removal efficiency of the system (Table 1). However, a shift in the K_{eq} for hydrogenolysis is observed, giving 1-chloro-2,2,2-trifluoroethane as the major product. Conversion of CCl_2FCClF_2 is similar to that for Pd/Zn ratios of 2 : 1 and 1 : 1, respectively, at 648 K, but an increase in the efficiency of the Pd/Zn = 1 : 2 system for hydrogenolysis is observed at 673 K at ca. 66%. Selectivity to 1,1,1-trifluoroethane is inversely proportion to temperature, with a corresponding increase in the selectivity to 1-chloro-2,2,2-trifluoroethane. For the Pd/Zn ratio = 1 : 2, the loss in selectivity to 1,1,1-trifluoroethane is 0.4 mol% K^{-1} over the temperature range 550–600 K, with selectivity to CH_3CF_3 increasing to 1.2 mol% K^{-1} at temperatures above 630 K. The accelerated loss in 1,1,1-trifluoroethane selectivity is again consistent with a restructuring of the catalyst surface or a formation of nonlabile adsorbates as a function of temperature and time-on-line. XPS analysis of the worked catalyst confirms an increase in the relative Pd^0/Al ratio by 48.5% (Table 1). The results show that a palladium enrichment of the catalyst occurs and is consistent with either a segregation process of the removal of the zinc component in the form of the halide.

DSC analysis of a freshly prepared sample of Pd/Zn ratio = 1 : 2 confirms that the addition of zinc to palladium renders the palladium resistant to oxidation relative to the Pd/γ-Al_2O_3 material in the temperature range 593–610 K. At temperatures between 446 and 590 K the material is more readily oxidised relative to the γ-alumina-supported palladium catalyst. Hydrogenolysis results for the Pd/Zn systems (Pd/Zn = 2 : 1; 1 : 1, and 1 : 2) operating over this temperature range show changes in the selectivity to the major product as a function of temperature and is consistent with surface restructuring. Studies at temperatures greater than 610 K confirm that selectivity to the major product reaches steady state conditions as a function of time.

An increase in the zinc component of the catalyst to give a Pd/Zn ratio of 1 : 4 produces a marked difference in the selectivity of the catalyst to give 1,1,1-trifluoroethane. In the temperature range 550–650 K, the selectivity to 1,1,1-trifluoroethane remained constant as a function of temperature and indicates that an enhanced stability in the structure of the catalyst surface exists relative to that of lower Pd/Zn ratios. A marked increase in the efficiency of removing chlorine is also observed, giving efficient chlorine hydrogenolysis at lower temperatures (Table 2). The addition of zinc to the palladium has an overall effect of shifting the chemical equilibrium of the surface reactions to hydrogenated products. Conversion of CCl_2FCClF_2 is measured at 83.9% with a selectivity to CH_3CF_3 of 93.8 mol%. Selectivity to chlorine products is low, with a measured chlorine removal efficiency of ca. 81.2%, an increase of 28-fold over Pd/γ-Al_2O_3.

The results show that the addition of zinc to palladium increases the selectivity of the catalyst to give hydrogenated products. The magnitudes of the equilibrium constants K_1, K_2, K_3, and K_4 are increased as a function of zinc content in palladium. The results are also consistent with the gas adsorption equilibria Λ_3 and Λ_4 tending to 0 and Λ_5 tending to ∞ as a function of increasing zinc content.

Chlorine mobility at palladium surfaces has been reported (48), and for the case of Pd–Zn couples we propose that chlorine mobility is enhanced by the presence of the reduced zinc function causing the surface coverage of chlorine at the palladium surface to remain low relative to that of γ-alumina-supported palladium. This hypothesis is based on the observation that the equilibrium for the hydrogenolysis reaction is moved to the right by the presence of zinc in the catalyst formulation pulling the selectivity of the catalyst through to hydrogenated products (Table 2, Fig. 3). The relatively low surface coverage of chlorine allows the equilibria at the surface to favour the formation of adsorbed hydrogen and chlorofluorocarbon substrate, respectively. Hydrogen spillover to the Pd–Zn couples allows the adsorbed chlorine species to desorb from the surface as hydrogen chloride. Hence the synergistic effect of the zinc function is to retard the formation of bulk palladium halides during the hydrogenolysis reaction, stabilising the catalyst under the severe oxidising conditions prevalent during the reaction. Hence, we can modify Eq. [1] to take into account the formation of hydrogen halide at a Pd–Zn junction:

$$\frac{d[CH_3CF_3]}{dt} = \frac{k_{\text{rate constant}} K_1 K_2 K_3 K_4 p_{CCl_2FCClF_2} p_{H_2}^{0.5}}{\left\{\left(1 + \Lambda_1 K_1 p_{CCl_2FCClF_2} + \Lambda_2 p_{H_2}^{0.5} + \Lambda_3 p_{CHCl_2CF_3} + \Lambda_4 p_{CH_2ClCF_3} + \Lambda_5 p_{CH_3CF_3}\right)\right\}^2 \times (\Lambda_p HF + \Lambda_6 p_{HCl})}. \quad [2]$$

Therefore the results from the hydrogenolysis are consistent with a Langmuir–Hinshelwood mechanism occurring at a dual site where the chlorofluorocarbon substrate and hydrogen are adsorbed species and hydrogen halide (chlorine or fluorine) formation occurring at a separate site location which is not available to chlorofluorocarbon adsorption.

Assuming that the hydrogenolysis CCl_2FCClF_2 to CH_3CF_3 occurs through the same series of transition states,

then the rate equation for the Langmuir–Hinshelwood bimolecular reaction is given by

$$\frac{-d[CCl_2FCClF_2]}{dt} = \frac{N_{CCl_2FCClF_2}}{V} \times \frac{N_{H_2}}{V} \times \frac{N_{\text{single sites}}}{A} \times \frac{kT}{h} \times \frac{q^{\#}}{q_{113}q_{H_2}q_{ss}} \cdot e^{-E_0/kT}, \quad [3]$$

where N is the number of CCl_2FCCl_2F, H_2, and single sites, respectively; V is the unit volume; A is the metal area; $q^{\#}$, q_{113}, q_{H_2}, q_{ss} are the partition functions for the transition state, CCl_2FCCl_2F, dihydrogen, and single sites, respectively; and k is the Boltzman constant.

Therefore $[N_{CClF_2CClF_2}/A]$, $[N_{H_2}/A]$, and $[N_s/A] = [N_{tot}/A]$ are the concentration of CCl_2FCClF_2, dihydrogen adsorption, and vacant single sites, respectively, at the catalyst surface. Then the rate at dual sites can be expressed as

$$\frac{-d[CCl_2FCClF_2]}{dt} = \frac{0.5[N_{CCl_2FCClF_2}/A][N_{H_2}/A][N_{tot}/A]}{\left(1 + K[N_{113}/V] + K[N_{H_2}/V]\right)^2} \times \frac{kT}{h} \times \frac{q^{\#}}{q_{113}q_{H_2}q_{ss}} \cdot e^{-E_0/kT}. \quad [4]$$

It is seen from the above that as the surface coverage tends to zero the expression reduces to give second order. However, the rate equation does not explain why the addition of zinc metal to palladium moves the equilibria for the reaction through to fully dechlorinated products.

Applying the principle of detailed equilibrium for a closed system, at equilibria nodes where the equilibrium constant for the step is positive (and given the assumption that nonequilibrium behaviour prior to and following equilibrium is simple and does not greatly effect the value of the equilibrium constant at a given node), by vector analysis,

$$\mathbf{\Gamma} \cdot \ln[\mathbf{N_{113}}/\mathbf{A}] = \ln \mathbf{K}, \quad \text{i.e., } \ln \mathbf{K} \in \mathrm{Im}\,\mathbf{\Gamma},$$

where $\mathbf{\Gamma}$ is the stoichiometric matrix for the hydrogenolysis of 1,1,2-trichlorotrifluoroethane to 1,1,1-trifluoroethane. However, the stoichiometric matrix elements are the same for each catalyst allowing that the formation of the observed products go through the same reactive intermediate species (49). Therefore the introduction of zinc to palladium effects the vector $\ln[\mathbf{N}_{113}/A]$ which is in effect equivalent to the term involving the partition function for the reactions $q^{\#}/(q_{113} \cdot q_{H_2} \cdot q_{ss})$. We have seen that the addition of zinc to the palladium results in an increase of the metal dispersion and hence an increase in the palladium–zinc junctions. As the average metal particle volume diminishes the relative density of steps and corners increases in conjunction with the simultaneous increase in Pd−Zn junctions. The change in the partition coefficients relating to adsorbed species and the subsequent shift of the K_{eq} for the reaction thus lie in the increase in high-energy adsorption sites generated from an increase in step and/or corner density together with the corresponding increase in the Pd−Zn concentration at these sites. Therefore the results are consistent with the dissociative adsorption sites for 1,1,2-trichlorotrifluoroethane being steps or corner dual sites comprising palladium in close proximity to zinc. The dissociated chlorine from 1,1,2-trichlorotrifluoroethane, being mobile at the reaction temperature, is adsorbed and subsequently hydrogenated at a Pd−Zn junction, leaving as gaseous hydrogen chloride.

CONCLUSIONS

The selectivity of a γ-alumina-supported palladium catalyst for the hydrogenolysis of 1,1,2-trichlorotrifluoroethane to hydrogenated products is greatly enhanced by the addition of zinc to the palladium function. The addition of zinc results in an increased dispersion of the palladium metal particles and stabilises the palladium function against the formation of bulk palladium chloride or fluoride and the subsequent catalyst deactivation XRD, DSC, and XPS analyses are consistent with the formation of a palladium–zinc alloy. Kinetic analysis reveals that the presence of the Pd−Zn couples is important by modifying equilibrium coverages of the adsorbed chlorofluorocarbon and halohydrocarbon species at a dual surface site comprising palladium in close proximity to zinc.

ACKNOWLEDGMENTS

We thank Mr. John D. Paton, Department of Chemistry, University of Dundee, for obtaining the XRD data. The authors also thank the University of Dundee, the Royal Society of Chemistry, and Durham Chemicals plc., Durham, England, for their financial support of this work.

REFERENCES

1. Manzer, L. E., and Rao, V. A., *Adv. Catal.* **39**, 329 (1993).
2. Holloway, J. H., Hope, E. G., Powell, R. L., and Townson, J., Eur. Pat. Appl., No. 92,301532.5 (1992).
3. Takita, Y., Yamada, H., Hashida, M., and Ishihara, T., *Chem. Lett.*, 715 (1990).
4. Tomioka, S., Kurokawa, H., Ueda, W., Morikawa, Y., and Ikawa, I., Prep. Fall Meeting, Catal. Soc. Japan, 3c31, 1989.
5. Bickelhaupt, F. M., Baerends, E. J., Nibbering, N. M. M., and Ziegler, T., *J. Am. Chem. Soc.* **115**(20), 9160 (1993).
6. Vanlauten, N., Wilmet, V., Pirotton, J., and Lerot, L., Eur. Pat. Appl. No. 556,893 (1993).
7. Coulson, D. R., *J. Catal.* **142**(1), 289 (1993).
8. Thomson, J., *Catal. Lett.* **40**, 119 (1996).
9. Sweetman, M. J., and Thomson, J., *J. Chem. Soc. Chem. Commun.*, 2385 (1994).
10. Thomson, J., Eur. Pat. Appl., No. 94909183.9 (1996).
11. Thomson, J., U.S. Pat. Appl., No. 08/507,488 (1996).
12. Thomson, J., U.S. Pat. Appl., No. 08/290,896 (1995).
13. Thomson, J., Internl. Pat. Appl., No. PCT/GB94/00477 (1994).
14. Thomson, J., *J. Chem. Soc. Faraday Trans.* **90**, 3585 (1994).
15. Ichikawa, M., Ohnishi, R., and Suzuki, H., Eur. Pat. Appl., No. 0459 463 A1 (1991).
16. Ichikawa, M., Ohnishi, R., and Suzuki, H., Jpn. Pat., No. 143053/90.
17. Ichikawa, M., Ohnishi, R., and Suzuki, H., Jpn. Pat., No. 143054/90.
18. Ichikawa, M., Ohnishi, R., and Suzuki, H., Jpn. Pat., No. 241691/90.

19. Ichikawa, M., Ohnishi, R., and Suzuki, H., Jpn. Pat., No. 241692/90.
20. Saliki, T., Sumida, M., Nakano, N., and Murakami, K., Eur. Pat. Appl., No. 0471320 A1.
21. Saliki, T., Sumida, M., Nakano, N., and Murakami, K., Jpn. Pat., No. 214113/90.
22. Darragh, J. I., U.K. Pat., No. 1578933 (1980).
23. Morikawa, S., Samejima, S., Yositake, M., and Tatematsu, S., Eur. Pat. Appl., No. 0347830 (1989).
24. Morikawa, S., Samejima, S., Yositake, M., and Tatematsu, S., Jpn. Pat., No. 39206/89.
25. Moore, G. J., and O'Kell, J., Eur. Pat. Appl., No. 0508660 A1.
26. Moore, G. J., and O'Kell, J., GB Pat., No. 9107677 (1991).
27. Nakada, T., and Koyama, S., Eur. Pat. Appl., No. 0587896 A1 (1992).
28. Nakada, T., and Koyama, S., Jpn. Pat., No. 307597 (1991).
29. Nakada, T., and Koyama, S., Jpn. Pat., No. 320324 (1991).
30. Coq, B., Cognion, J. M., Figueras, F., and Tournigant, D., *J. Catal.* **141**, 21 (1993).
31. Gervasutti, C., Marangoni, L., and Parra, W., *J. Fluorine Chem*. **19**, 1 (1981).
32. Takita, Y., Yamada, H., Ishihara, T., and Mizuhara, Y., *Nippon Kagaku Kaishi*, 594 (1991).
33. Takita, Y., Yamada, H., Ishihara, T., and Mizuhara, Y., *Chem. Lett.*, 715 (1990).
34. Clark, J. W., U.S. Pat., No. 2,685,606 (1954).
35. Ward, J. A., U.S. Pat., No. 3,927,131 (1975).
36. Gervasutti, C., Eur. Pat., No. 0253410 (1987).
37. Keller, C. S., and Mallikarjuna, V. N., U.S. Pat., No. 4873381 (1989).
38. Fitzgerald, A. G., Moir, P. A., and Storey, B. E., *J. Electron Spectrosc. Relat. Phenomen.* **59**, 127 (1992).
39. ASTM Crystal Data Determination Tables.
40. Williams, G. P., National Synchroton Light Source, Brookhaven Natl. Lab., Upton, NY.
41. X-Ray Powder Data File, ASTM-6-0620.
42. Nag, N. K., *Catal. Lett.* **24**, 37 (1994).
43. Briggs, D., and Seah, M. P. (Eds.), "Practical Surface Analysis by Auger and X-Ray Photoelectron Surface Analysis." Wiley, Chichester, 1985.
44. Pitehon, V., Guenin, M., and Praliaud, H., *Appl. Catal.* **63**, 333 (1990).
45. Thomson, J., unpublished data.
46. Carpenter, G. B., "Principles of Crystal Structure Determination." Benjamin, Elmsford, NY, 1969.
47. Rowley, L., Thomson, J., Webb, G., Winfield, J. M., and McCulloch, A., *Appl. Catal.* **79**, 347 (1991).
48. Campbell, J. S., and Kemball, C., *Trans. Faraday Soc.* **59**, 2583 (1963).
49. Compton, R. G. (Ed.), "Kinetic Models of Catalytic Reactions," Vol. 32. Elsevier, New York, 1991.